How to cite: *Angew. Chem. Int. Ed.* **2023,** *62,* e202212724
International Edition: doi.org/10.1002/anie.202212724
German Edition: doi.org/10.1002/ange.202212724

Circularly Polarized Luminescence

Strong Coupling of Chiral Frenkel Exciton for Intense, Bisignate Circularly Polarized Luminescence

*Minghao Li[+], Shahana Nizar[+], Sudipta Saha, Anoop Thomas, Stefano Azzini, Thomas W. Ebbesen, and Cyriaque Genet**

Abstract: We show that chiral Frenkel excitons yield intense circularly polarized luminescence with an intrinsic dissymmetry factor in emission g_{lum} as high as 0.08. This outstanding value is measured through thin films of cyanine *J*-aggregates that form twisted bundles. Our measurements, obtained by a Mueller polarization analysis, are artifact-free and reveal a quasi-perfect correlation between the dissymmetry factors in absorption, g_{abs}, and in emission g_{lum}. We interpret the bisignate dissymmetry factors as the signature of a strong coupling between chiral Frenkel excitons longitudinally excited along the bundles. We further resolve by polarimetry analysis the split in energy between the excited states with a Davydov splitting as small as 28 meV. We finally show the anti-Kasha nature of the chiral emission bands with opposite optical chirality. These mirror-imaged emissive chiroptical features emerge from the structural rigidity of the bundles that preserves the ground- and excited-state chirality.

Introduction

The recent focus put on circularly polarized luminescence (CPL) is driven both by fundamental and applied perspectives.[1–3] Fundamentally, CPL offers a unique way of probing the chiroptical features of molecular excited states, and for understanding how these features emerge from and interact with, the stereochemical structure of chiral molecules.[4,5] From an applied perspective, the possibility to tailor polarization dissymmetry of light emitting systems contributes to the definition of novel optical technologies, where for instance CPL plays a key role for enhancing the contrast of conventional organic light-emitting diode displays and thereby their energy efficiency, for the development of chiral lasers, all-optical information processing strategies, chiral microscopy and for chiral sensing.[6–13]

The strength of CPL is determined by the luminescence dissymmetry factor, $g_{lum}=2(I_L-I_R)/(I_L+I_R)$ where I_L and I_R are the left- and right-handed emission intensities. In the small molecule (i.e. dipolar) limit, dissymmetry factors are usually bounded to 10^{-5}–10^{-3} by a low ratio between the electric and the magnetic transition dipole moments.[15–18] Chiral lanthanide complexes are well known exceptions with g_{lum} reached by magnetic-dipole allowed and electric-dipole reduced transitions whose weakly emissive nature is compensated by the use of ligands acting as antennas.[19–21]

In addition to exploiting and engineering dipole forbidden transitions, chiral aggregation is another well-identified route to enhance CPL since it facilitates exciton coupling mechanisms that are known to strengthen chiroptical responses.[22–24] Through aggregation, (as for instance in the case of *J*-type aggregates), neighboring chromophores become strongly coupled and the excitation is delocalized among them. With such delocalized Frenkel excitons, the effective size of the active chiral component associated with the aggregated molecular system can be increased, resulting in amplified g_{lum} values. The aggregation, however, is very often accompanied by strong fluorescence quenching due to the formation of excimers/exciplexes or to dipole forbidden induced transitions. Unfortunately, therefore, testing the impact of aggregation on CPL remains a difficult task, despite recent strategies that have proposed new families of solid, chiral emitters capable of intensively emitting once aggregated in the condensed phase.[25,26]

Another key feature of luminescent rigid aggregates is their sharp emission lines with reduced Stokes shifts that correspond to minimal conformational relaxation from the excited to the ground states. This implies a strong correlation between the states where the chiroptical features of the

[*] M. Li,[+] S. Nizar,[+] S. Saha, A. Thomas, S. Azzini, T. W. Ebbesen, C. Genet
CNRS, CESQ-ISIS, University of Strasbourg, UMR 7006
67000 Strasbourg (France)
E-mail: genet@unistra.fr
M. Li[+]
Quantum Sensing Laboratory, Department of Physics, University of Basel (Switzerland)
A. Thomas
Inorganic and Physical Chemistry, Indian Institute of Science Bengaluru (India)
S. Azzini
Nanoscience Laboratory, Department of Physics, University of Trento (Italy)
[+] These authors contributed equally to this work.

ground state -probed through the molecular circular dichroism (CD)- are in direct relation with the chiroptical features of the excited states measured by CPL. Therefore, in such condensed aggregated phases, the concomitant occurrence of exciton delocalization and the ground-to-excited states correlation is expected to yield large g_{lum} enhancement effects. Despite this important expectation, experiments have been scarce.[4]

In this Article, we demonstrate that among the various classes of organic self-assemblies, chiral tubular aggregates formed by the spontaneous self-assembly of π-stacked achiral amphiphilic C8O3 (3,3′-bis(3-carboxy-n-propyl)-3,3′-di-n-octyl-5,5′,6,6′-tetrachlorobenzimidacarbocyanine) cyanine dyes yield intense CPL with measured g_{lum} values as high as 0.08. This demonstration complements and confirms, from the excited state view point, the extraordinary chiroptical features of such C8O3 cyanine Frenkel excitons that emerge through self-assembly, following the strict hierarchical evolution of chirality schematized in Figure 1a–d that we studied in detail.[27] By resorting to artifact-free Mueller polarimetry, we are able to reveal the quasi-perfect ground-to-excited state correlation and unveil the bisignate profile of this intense CPL distributed in two narrow spectral bands of opposite helicities. These results lead us to explain the g_{lum} profile and amplitude as consequences of the strong coupling induced between the chiral Frenkel excitons when the tubular aggregates get intertwined into large, twisted bundles in the very last chiral nucleation stage of the self-assembly.

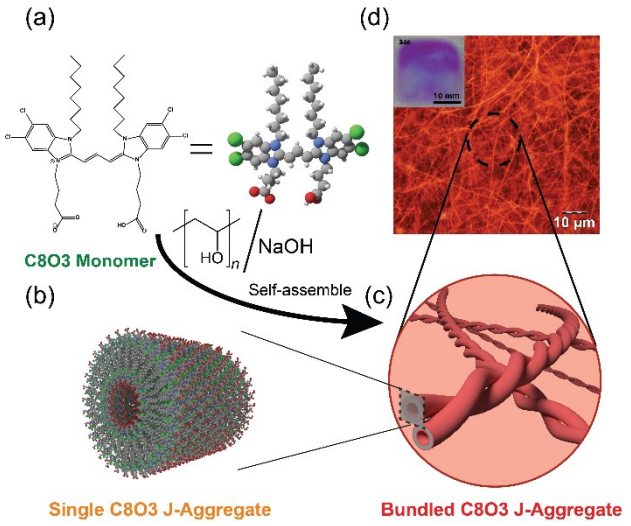

Figure 1. a) Chemical structure of the amphiphilic C8O3 dye monomer that self-assembles in chiral, double-layer tubular aggregates in film, sketched in (b), formed by adding a mixture of PVA and NaOH water solution into the monomer solution prepared with ethanol.[14] c) In a late stage of the self-assembly, the tubular aggregates get intertwined in the twisted bundles our work focuses on, and that can directly be imaged using dark-field microscopy (d) of the C8O3 self-assembled in thin films. The inset in (d) shows a typical photograph of the thin film sample as it appears after preparation.

Results and Discussion

We start by showing in Figure 2a the optical properties of the cyanine achiral monomers measured in a solution of 6 % PolyVinylAcetate (PVA) and 10 mM NaOH solution mixed with 0.25 mM C8O3 solution in Ethanol in a 1:1 volume ratio. UV/Vis absorption and photoluminescence spectra of the monomers are shown in Figure 2a, displaying an absorption peak of the monomers at 530 nm and an emission peak, Stokes-shifted by ca. 20 nm. As expected from the achiral nature of the monomers, the solution does not show chiroptical features.[27]

In the condensed phase, aggregation is induced following the methodology proposed in ref. [28] with the solution drop-casted on a glass substrate and kept overnight for drying. A thin film of (1–4) μm thickness is formed within which chiral C8O3 aggregates grow (see the picture in the top left corner of Figure 1d). Such thin films are strongly inhomogeneous, as seen in the dark-field microscope image of Figure 1d, which clearly reveals the complexity of the film, with C8O3 monomeric domains coexisting with other

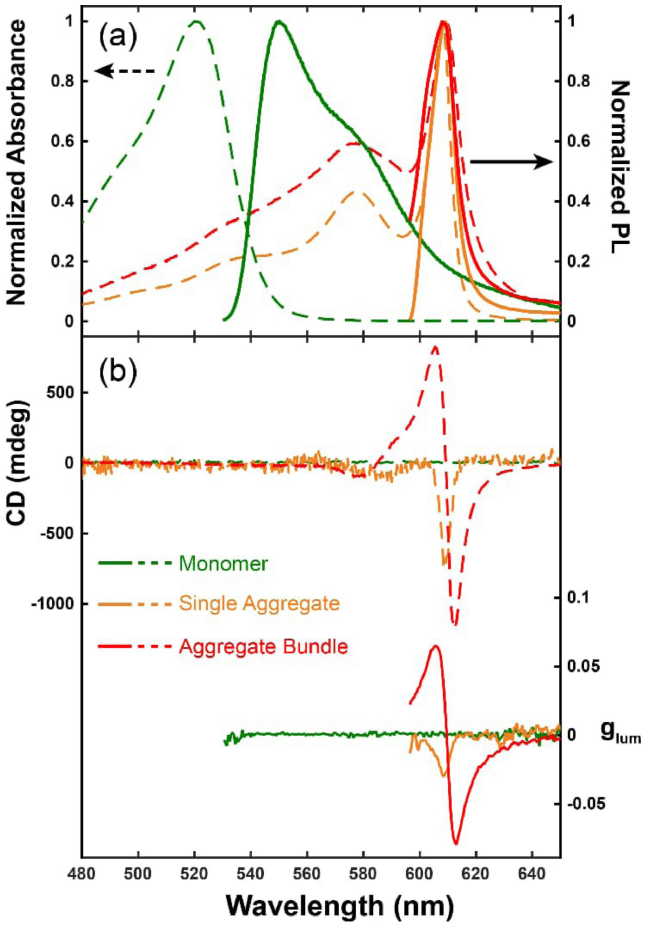

Figure 2. a) Normalized absorption (dotted lines) and normalized emission (solid lines) spectra of C8O3 monomers in solution (green), single tubular aggregate (orange) shown in Figure 1b, and aggregate bundle (red) shown in Figure 1c. b) The CD and CPL dissymmetry factor g_{lum} for each of these 3 conformations.

domains that are fiber-textured by the tubular C8O3 aggregates.

To measure the optical response of the aggregates, it is important to use microscope objectives that enable us to record optical spectra within a reduced field of view over which the region of interest (ROI) is almost homogeneous. By doing so, we record the absorption spectrum of the C8O3 aggregates and identify in Figure 2a the absorption peak of the longitudinal exciton at 610 nm and the transverse exciton at 576 nm. When measuring the absorption, we took great care to adjust the power of the probing white light source to minimize any spectral contribution that, otherwise, could come from uncontrolled emission. To do so, we monitored and minimized the emission signal through all absorption experiments and minimized it using cross-polarizers. Using long-pass optical filters (see Supporting Information file for details) the photoluminescence spectrum is also recorded with a sharp emission peak at 610 nm and practically zero Stokes shift, i.e. an emission spectrum typical of *J*-type π-stacked aggregates of the monomers.

As seen in Figure 1b, the aggregates in the thin film form domains that are strongly anisotropic due to the high aspect ratio of the helical tubular shape of the aggregated assemblies. In such anisotropic domains, the polarization signatures of the chiral tubular aggregates must be assessed with care, considering that the unavoidable and large linear dichroism and linear birefringence of the film can spoil, as artifacts, the measure of the CD of the aggregates. This issue in absorption is the same in emission, where linearly polarized luminescence (LPL) can contribute to and bias CPL measurements (see below). To access artifact-free chiroptical features, and in particular here CD spectra, we use a comprehensive Mueller polarimetry analysis (see for instance ref. [29] and references therein). This analysis is capable of canceling the influence of the high anisotropy of the assemblies on the determination of their intrinsic chiral responses, which is the case at all stages of aggregation.

The growth of C8O3 aggregates proceeds through the symmetry breaking mechanism we described in ref. [27]. This breaking of symmetry leads to a high enantiomeric excess within the aggregate ensemble, as seen from the fixed sign of the Cotton effect observed in the measured CD spectra -see Figure 2b. Then, bundles of such enantiomer aggregates are formed, but the twist adopted by the bundling can a priori be either left-handed (*M*-form of chirality) or right-handed (*P*-form) with no chiral selectivity at this last stage of aggregation. Microscope objectives serve an important purpose here as they give the possibility of spatially selecting individual bundle enantiomers among this racemic mixture and recording, at the few-single-bundle level, their CD and CPL spectra.

We first measure the absorption spectrum of a single bundles. The spectrum shown in Figure 2a reveals that the absorption peak of the longitudinal exciton of the bundle is slightly blue shifted (ca. 2 nm), a shift to be associated with the inter-aggregate interactions of the longitudinal excitons along the bundle. We then compare, selecting with the objective different ROI on the film, the CD spectra associated with the tubular aggregates and the single bundles of aggregates, respectively. The CD spectrum of tubular aggregates is, surprisingly, characterized by a single negative peak (see Figure 2b, orange curve) while one would have expected a positive counterpart. This observation certainly deserves further attention and might stem from some additional, yet unresolved, weak chiral signals that contribute to canceling the high energy part of the expected bisignate CD, leaving only a single, negative, low energy contribution to the CD spectrum of the tubular aggregate.

In contrast, the CD spectrum associated with the bundles is clearly bisignate, with a crossover at 608 nm, i.e. at the maximal absorption of the longitudinal exciton, see Figure 2a, b. As we will discuss further down, this bisignation is the signature of the strong coupling between longitudinal Frenkel excitons of one C8O3 aggregate and another, induced through the formation of the bundles.

We verified the stochastic distribution of *P*- vs. *M*-forms of chirality for the bundles by measuring the sign-exchange of bisignation at different (18) locations picked up on thin film samples using microscope objectives. The results of 10 measurements associated with the *M*-form and 7 with the *P*-form are displayed in Figure 3c (These 17 CD measurements are shown in Supporting Information). This nearly statistical distribution of forms reveals the racemic nature of the ensemble of bundles formed with both handednesses within the film.

These high CD values measured for the bundle ground states led us to probe the chiroptical features of the corresponding excited states and to measure the CPL values associated with both the C8O3 aggregates and bundles. To do so, we took great care in distinguishing the *intrinsic* molecular g_{lum} dissymmetry factor from the strong LPL contributions unavoidably induced by the high anisotropy of our samples. To provide artifact-free CPL values, it is therefore necessary here too to resort to Mueller polarimetry. We thus measured CPL spectra by fluorescence Mueller polarimetry, where the g_{lum} dissymmetry factor reads directly from one specific coefficient of the Mueller matrix, as explained in the Supporting Information file.

This notion of *intrinsic* CPL is central to our work and requires special attention with respect to the fact that the PL emission spectrum overlaps with the absorption spectrum of the longitudinal *J*-band, as shown in Figure 2a. This causes CPL measurements to be potentially modified by a filtering effect due to the transmission of the emitted photons through the linear dichroic, linear birefringent and circular dichroic thin film itself.[26,30] Therefore, the modifications imprinted by this filtering effect must be carefully accounted for to access the intrinsic molecular CPL. Correcting for this filtering effect on our measurements can be done by exploiting Mueller polarimetry again, as we explain in detail in the Supporting Information file.

The PL measurements are performed by exciting the sample from 510 nm to 580 nm with 8 nm step size in wavelength, and the corresponding normalized emission spectra are presented in Figure 4a. They show the emission intensity decreasing with the excitation wavelength, just like absorbance does. We measure in Figure 4b the CPL dissymmetry factor g_{lum} throughout this excitation band-

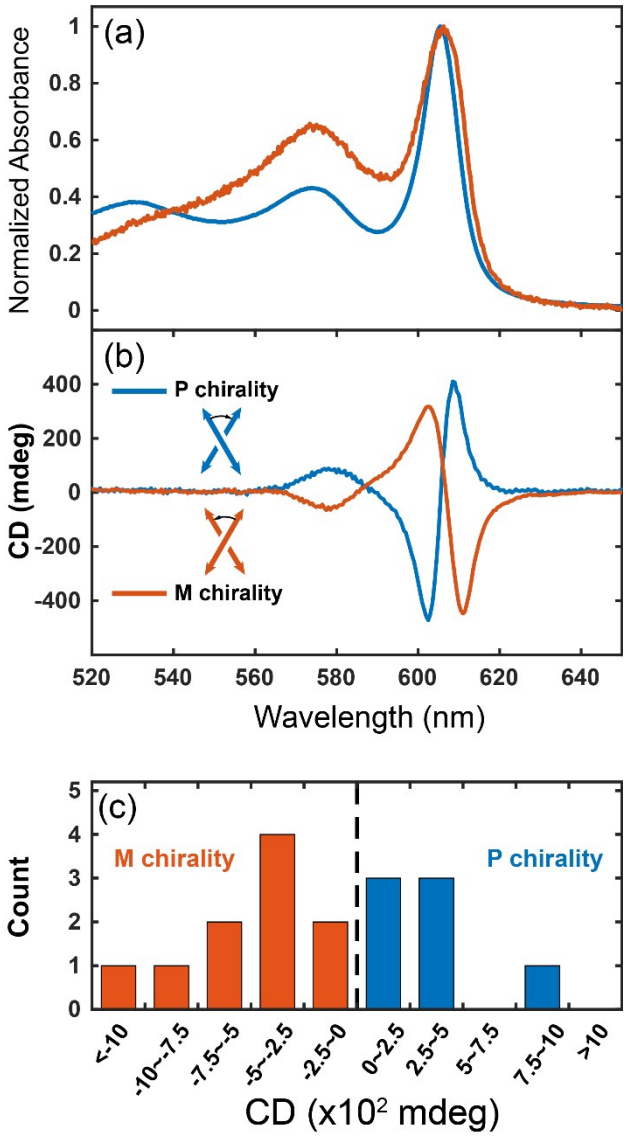

Figure 3. a) Absorption spectra associated with each *P*- and *M*-forms of chirality for the twisted bundles self-assembled in the thin film of C8O3 in PVA/NaOH. b) Corresponding artifact-free CD spectra measured using Mueller polarimetry. Note that the crossover points of bisignate CD are both right on the superimposed absorption peak of each form. c) Statistical distribution of *P*- and *M*-forms through the thin film, revealing no particular bias, thereby characterizing the racemic nature of the thin film as far as bundle formation is concerned.

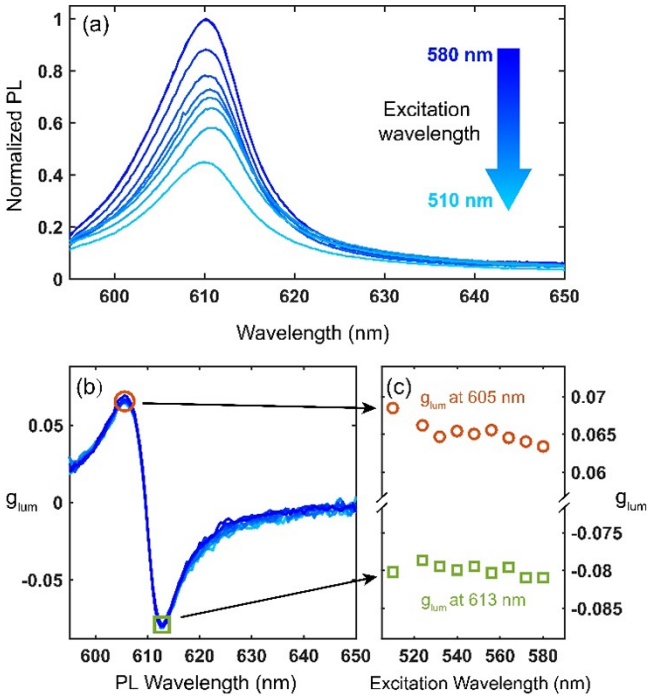

Figure 4. a) Normalized photoluminescence (PL) and b) g_{lum} spectra of C8O3 bundles excited with wavelengths ranging from 580 nm to 510 nm (510 nm, 524 nm, 532 nm, 540 nm, 548 nm, 556 nm, 564 nm, 572 nm, 580 nm). The inset in (a) details where the excitation wavelengths (all within the blue area) sit in the absorption and CD spectra. c) The CPL excitation (CPLE) spectra is built by monitoring the evolution of the g_{lum} extremum values (at 605 nm and 613 nm) of the bisignate CPL throughout the excitation bandwidth.

width that keeps its bisignate profile constant for all excitation wavelengths with the same crossover at the emission maxima. We then display in Figure 4c the CPL excitation (CPLE) spectrum where both the maxima (positive) at 605 nm and the minima (negative) at 613 nm of the g_{lum} bisignate spectra are plotted as a function of excitation wavelength. This CPLE spectrum demonstrates that the chiral molecular system radiatively relaxes from the same electronic excited states regardless of the excitation energy. As one central result of this work, the intrinsic, artifact-free, g_{lum} factor measured from the film reached a remarkably high value of 0.08, demonstrating how the chirality in emission is further enhanced by the coupling of longitudinal chiral aggregate Frenkel excitons through the bundle formation.

To further emphasize these exceptional features, we looked at the correlation between the CD and CPL spectra, i.e. the correlation between the ground and the excited state chirality. The correlation appears very clear in Figure 5a, b near the longitudinal exciton transition, with identical magnitudes and signs for g_{abs} and g_{lum}. The correlation can be quantified by plotting g_{lum} against g_{abs} for wavelengths within the absorption vs. emission overlapping spectral range (orange area in Figure 5c). The values, collected from 4 different samples, are distributed linearly along a line of slope 1 going through the origin, assessing the nearly perfect correlation between g_{abs} and g_{lum}.

In general, such correlations, when observed, are weaker for the vast majority of chiral organic molecules with $g_{lum} < g_{abs}$. This reduction in the correlation is due to conformational flexibility and internal relaxations through the vibrational manifolds as manifested by non-negligible Stokes shifts.[4] For our bundles of *J*-aggregates, the high correlation essentially stems from the near-zero Stokes shift, implying that the transition engaged in the absorption (excitation) and emission processes is the same. This immediately forces the g_{abs} factor to be equal to the g_{lum} factor, since each factor can be expressed as $g = 4R/D$ where R is the rotational

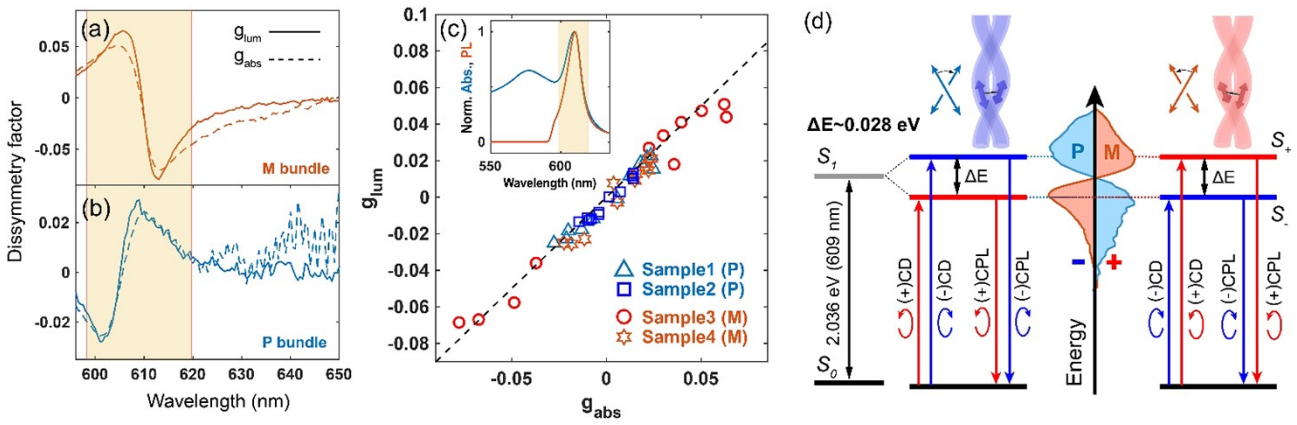

Figure 5. Absorption and emission dissymmetry factors g_{abs} and g_{lum} for bundles of a) *P*- and b) *M*-forms of chirality. c) Correlation of g_{abs} and g_{lum} for different samples in the *M*- and *P*-forms, gathering data from 4 different samples and bisignate profiles of different amplitudes. Data points are taken for each sample at 10 different wavelengths within the overlapping wavelength range for absorption and emission spectra (orange area, data taken from 596 nm to 620 nm with a 2.4 nm increment). The dashed line with a slope 1 clearly shows the quasi-perfect correlation between g_{abs} and g_{lum}. d) Jablonski energy diagrams built from the CD, CPL, and CPLE measurements, each associated with *M*- and *P*-forms of bundle chirality. The Frenkel exciton strong coupling yields a Davydov splitting of 28 meV for both forms.

strength and *D* the total dipolar strength of the ground-to-excited or excited-to-ground state transition, respectively. Evidently then, if the chirally active absorption and emission processes involve the same transition, both factors are identical, resulting in the quasi-perfect correlation that we measure.

Combining the CD and CPLE spectra in the light of this correlation puts us in the position to propose the energy level diagrams to be associated with the unique chiroptical features of the *P*- and *M*-forms of the bundles. The diagrams are sketched in Figure 5d. They are built adapting Kuhn's coupled dipole model to our case where the two strongly coupled dipoles consist of the chiral Frenkel excitons longitudinally excited along each tubular *J*-aggregate, obliquely intertwined together and thus forming the twisted bundle.[31] This type of arrangement between single tubular aggregate excitons in a bundle is well supported by the slight blue shift observed in the absorption spectrum of the bundles when compared to that of the single aggregates -see Figure 2a.

The oblique-type strong coupling[32] results in two new states for which the Frenkel excitons are coupled in-phase for the state S_+ and out-of-phase for the state S_-.[33,34] As such, both $S_\pm$ states display opposite chirality manifested by opposite optical spin angular momentum selection rules, in agreement with the respective signs of the measured CD (absorption) and CPL (emission) shown in Figure 5a, b. The enantiomeric relation between the *P*- and *M*-forms of the bundles observed from the comparison of the absorption vs. emission dissymmetry factors is perfectly reflected on the corresponding mirror-imaged energy level diagrams, and the bisignation give for both forms identical 28 meV Davydov splitting, i.e. identical inter-Frenkel exciton coupling strength. With such a small Davydov splitting, we stress that these two $S_\pm$ states are indiscernible by simply looking at absorption or emission spectra. Only a polarimetry analysis resolves the split excited states of the two strongly coupled aggregate excitons at room temperature.

The CPLE spectra of Figure 4c clearly show that the excitation to high energy states relaxes down the two new states $S_\pm$ and that emission occurs from both. The emissive nature of the S_+ state is remarkable and corresponds to an anti-Kasha relaxation dynamics not expected in most emissive molecular systems in the condensed phase.[35–37] The S_+ state is populated from higher excited states after laser excitation. But considering that the 28 meV Davydov splitting is just of the same order of the 25 meV thermal energy available to our system at room temperature (300 K), it can also be populated from the S_- state according to Boltzmann distribution law. The dense π-π stacking of monomeric units in the bundled J-aggregates that quenches internal relaxation paths then favors the emissive nature of the S_+ state. This reduction of non-radiative decay channels in the S_+ state is confirmed by an increase in photoluminescence efficiency (as presented in the Supporting Information file) and by the perfectly overlapping bisignate profiles observed in Figure 5a, b. These overlapping profiles demonstrate how chiral light absorption and emission both occur from the two new states $S_\pm$, in agreement with the energy diagram proposed in Figure 5d.

Conclusion

In summary, we have investigated the ground and the excited state chiroptical properties of bundles of C8O3 aggregates in thin film. Such aggregates were not previously identified as potential CPL emitters, but focusing specifically on the chiral bundles that form in the latest aggregation stage, we identified bisignation in both the ground and the excited state chiroptical signals originating from the chiral exciton coupling of longitudinal electronic transition in single tubular aggregate. By performing emission Mueller

polarimetry, we have obtained an artifact-free CPL signal with a high absolute g_{lum} of the order of 0.08 from bundles of C8O3 aggregates. We stress that our Mueller polarimetry has been essential for accessing chiroptical properties that are otherwise hardly accessible through conventional optical methodologies when aiming at characterizing CPL emitters with low Stokes shift and large anisotropies.

We then measured the dissymmetry factors in absorption and in emission that showed nearly 100 % one-to-one correlation with overlapping g_{abs} and g_{lum} spectra near the longitudinal absorption cross-section. This correlation indicates high chirality preservation in the ground and the excited states. Along with these highly correlated chiral signals, anti-Kasha emissive features emerged from the structural rigidity of the bundles that preserves the ground and excited state chirality and thus yields mirror imaged spin angular momentum selection rules. These properties turn C8O3 twisted bundles of chiral Frenkel excitons into a promising chiroptical material. Their capacity to yield opposite chiral emissive bands with high contrast and within a very narrow bandwidth (associated with the small 28 meV Davydov splitting) opens fascinating opportunities for exploiting such supramolecular systems in complex chiral photonic architectures.

Acknowledgements

This work of the Interdisciplinary Thematic Institute QMat, as part of the ITI 2021 2028 program of the University of Strasbourg, CNRS and Inserm, was supported by IdEx Unistra (ANR-10-IDEX-0002) and by SFRI STRATUS project (ANR-20-SFRI-0012), and by ANR Equipex Union (ANR-10-EQPX-52-01), the Labex CSC (ANR-10-LABX-0026-CSC), the Labex NIE (ANR-11-LABX-0058-NIE) and USIAS (ANR-10-IDEX-0002-02) under the framework of the French Investments for the Future Program. The data that support the findings of this study are available within the paper and its Supporting Information files. Additional data and file are available from the corresponding authors upon reasonable request.

Conflict of Interest

The authors declare no conflict of interest.

Data Availability Statement

The data that support the findings of this study are available within the paper and its Supporting Information files. Additional data and file are available from the corresponding authors upon reasonable request.

Keywords: Chirality · Circularly Polarized Emission · Exciton Coupling · Mueller Polarimetry · Self-Assembly

[1] K. Dhbaibi, L. Favereau, M. Srebro-Hooper, C. Quinton, N. Vanthuyne, L. Arrico, T. Roisnel, B. Jamoussi, C. Poriel, C. Cabanetos, J. Autschbach, J. Crassous, *Chem. Sci.* **2020**, *11*, 567.
[2] J. L. Greenfield, J. Wade, J. R. Brandt, X. Shi, T. J. Penfold, M. J. Fuchter, *Chem. Sci.* **2021**, *12*, 8589.
[3] J. Kumar, T. Nakashima, T. Kawai, *J. Phys. Chem. Lett.* **2015**, *6*, 3445.
[4] H. Tanaka, Y. Inoue, T. Mori, *ChemPhotoChem* **2018**, *2*, 386.
[5] E. S. Gauthier, L. Abella, N. Hellou, B. Darquié, E. Caytan, T. Roisnel, N. Vanthuyne, L. Favereau, M. Srebro-Hooper, J. G. Williams, J. Autschbach, J. Crassous, *Angew. Chem. Int. Ed.* **2020**, *59*, 8394; *Angew. Chem.* **2020**, *132*, 8472.
[6] K. Dhbaibi, L. Abella, S. Meunier-Della-Gatta, T. Roisnel, N. Vanthuyne, B. Jamoussi, G. Pieters, B. Racine, E. Quesnel, J. Autschbach, J. Crassous, L. Favereau, *Chem. Sci.* **2021**, *12*, 5522.
[7] S. Furumi, *Chem. Rec.* **2010**, *10*, 394.
[8] D. Qu, M. Archimi, A. Camposeo, D. Pisignano, E. Zussman, *ACS Nano* **2021**, *15*, 8753.
[9] B. L. Feringa, R. A. van Delden, N. Koumura, E. M. Geertsema, *Chem. Rev.* **2000**, *100*, 1789.
[10] M. Schulz, F. Balzer, D. Scheunemann, O. Arteaga, A. Lützen, S. C. Meskers, M. Schiek, *Adv. Funct. Mater.* **2019**, *29*, 1900684.
[11] S. Huang, H. Yu, Q. Li, *Adv. Sci.* **2021**, *8*, 2002132.
[12] F. Song, G. Wei, X. Jiang, F. Li, C. Zhu, Y. Cheng, *Chem. Commun.* **2013**, *49*, 5772.
[13] C. Zhang, X. Wang, L. Qiu, *Front. Chem.* **2021**, *9*, 711488.
[14] U. De Rossi, S. Dähne, S. C. Meskers, H. P. Dekkers, *Angew. Chem. Int. Ed. Engl.* **1996**, *35*, 760; *Angew. Chem.* **1996**, *108*, 827.
[15] T. Amako, T. Kimoto, N. Tajima, M. Fujiki, Y. Imai, *Tetrahedron* **2013**, *69*, 2753.
[16] N. Saleh, M. Srebro, T. Reynaldo, N. Vanthuyne, L. Toupet, V. Y. Chang, G. Muller, J. G. Williams, C. Roussel, J. Autschbach, J. Crassous, *Chem. Commun.* **2015**, *51*, 3754.
[17] K. Dhbaibi, L. Favereau, M. Srebro-Hooper, M. Jean, N. Vanthuyne, F. Zinna, B. Jamoussi, L. Di Bari, J. Autschbach, J. Crassous, *Chem. Sci.* **2018**, *9*, 735.
[18] Y. Li, Q. Li, X. Miao, C. Qin, D. Chu, L. Cao, *Angew. Chem. Int. Ed.* **2021**, *60*, 6744; *Angew. Chem.* **2021**, *133*, 6818.
[19] J. L. Lunkley, D. Shirotani, K. Yamanari, S. Kaizaki, G. Muller, *J. Am. Chem. Soc.* **2008**, *130*, 13814.
[20] G. Muller, *Dalton Trans.* **2009**, 9692–9707.
[21] C. A. Mattei, K. Dhbaibi, B. Lefeuvre, V. Dorcet, G. Argouarch, O. Cador, B. Le Guennic, O. Maury, C. Lalli, S. Guy, *Chirality* **2022**, *34*, 34–47.
[22] Y. Deng, M. Wang, Y. Zhuang, S. Liu, W. Huang, Q. Zhao, *Light: Sci. Appl.* **2021**, *10*, 1.
[23] R. Tempelaar, A. Stradomska, J. Knoester, F. C. Spano, *J. Phys. Chem. B* **2011**, *115*, 10592.
[24] F. C. Spano, Z. Zhao, S. C. Meskers, *J. Chem. Phys.* **2004**, *120*, 10594.
[25] J. Liu, H. Su, L. Meng, Y. Zhao, C. Deng, J. C. Ng, P. Lu, M. Faisal, L. J. WY, X. Huang, H. Wu, K. S. Wong, B. Z. Tang, *Chem. Sci.* **2012**, *3*, 2737.
[26] G. Albano, G. Pescitelli, L. Di Bari, *Chem. Rev.* **2020**, *120*, 10145.
[27] A. Thomas, T. Chervy, S. Azzini, M. Li, J. George, C. Genet, T. W. Ebbesen, *J. Phys. Chem. C* **2018**, *122*, 14205.
[28] H. von Berlepsch, S. Kirstein, R. Hania, C. Didraga, A. Pugzlys, C. Böttcher, *J. Phys. Chem. B* **2003**, *107*, 14176.
[29] M. Li, *Mueller polarimetry for probing supramolecular and optical chiralities.* Physics [physics]. Université de Strasbourg, **2020**. English. (NNT : 2020STRAF018). (tel-03619839).

[30] G. Longhi, E. Castiglioni, J. Koshoubu, G. Mazzeo, S. Abbate, *Chirality* **2016**, *28*, 696.
[31] N. Berova, P. L. Polavarapu, K. Nakanishi, R. W. Woody, *Comprehensive Chiroptical Spectroscopy: Instrumentation, Methodologies, and Theoretical Simulations, Vol. 2*, Wiley, Hoboken, **2011**, pp. 115–126.
[32] M. Kasha, H. R. Rawls, M. A. El-Bayoumi, *Pure Appl. Chem.* **1965**, *11*, 371.
[33] K. Swathi, C. Sissa, A. Painelli, K. G. Thomas, *Chem. Commun.* **2020**, *56*, 8281.
[34] N. S. Nizar, M. Sujith, K. Swathi, C. Sissa, A. Painelli, K. G. Thomas, *Chem. Soc. Rev.* **2021**, *50*, 11208.
[35] G. Viswanath, M. Kasha, *J. Chem. Phys.* **1956**, *24*, 574.
[36] A. P. Demchenko, V. I. Tomin, P. T. Chou, *Chem. Rev.* **2017**, *117*, 13353.
[37] S. T. Duong, M. Fujiki, *Polym. Chem.* **2017**, *8*, 4673.

Manuscript received: August 30, 2022
Accepted manuscript online: November 25, 2022
Version of record online: December 28, 2022